Squeeze-out of nuclear matter as a function of projectile energy and mass

H.H. Gutbrod,[1,*] K.H. Kampert,[2] B. Kolb,[1,*]
A.M. Poskanzer,[3] H.G. Ritter,[3] R. Schicker,[3] and H.R. Schmidt[1,*]
[1] *Gesellschaft für Schwerionenforschung, D-6100 Darmstadt, West Germany*
[2] *University of Münster, D-4400 Münster, West Germany*
[3] *Nuclear Science Division, Lawrence Berkeley Laboratory, Berkeley, California 94720*
(Received 8 January 1990)

Squeeze-out, a component of the collective flow of nuclear matter, is the preferential emission of particles out of the reaction plane. Using the sphericity method the out-of-plane/in-plane ratio of the kinetic energy flow has been analyzed as a function of multiplicity and beam energy for Ca+Ca, Nb+Nb, and Au+Au collisions measured with the Plastic Ball detector at the Bevalac. Also, azimuthal distribution of the particles around the flow axis are presented together with the extracted out-of-plane/in-plane ratios. Finally, the rapidity dependence of the out-of-plane/in-plane ratio has been investigated with a new method using the transverse momentum components of the particles.

I. INTRODUCTION

A. The equation of state

The goal of global analysis of 4π data from relativistic nuclear collisions is to learn about the properties of highly compressed nuclear matter ($\varrho/\varrho_0 \geq 2$) and to extract information on its behavior under extreme conditions of high temperature and high baryon density. Ultimately, one would like to understand the nuclear equation of state, EOS, i.e., the response of the nuclear medium to these extreme conditions.

Probing the nuclear matter EOS in regions of high densities and temperatures ($\varrho/\varrho_0 \simeq 2$–5, T=50–100 MeV) is of fundamental importance not only in nuclear physics (nuclear viscosity, heat conductivity, possible phase transitions such as liquid-vapor, pion condensation, Δ isomers, etc.) and field theory (QCD phase transition to a quark-gluon plasma), but is also a basic prerequisite for an understanding of many astrophysical problems. For example, the dynamics of the early universe during the first fractions of a second after the "Big Bang," as well as the dynamics of supernova explosions and the structure and stability of neutron stars, depend strongly on the compressibility of nuclear matter[1-3] over wide regions of densities, temperatures, and Z/A ratios. Relativistic nuclear collisions are the first opportunity to study these phenomena under controlled conditions in the laboratory.[4-6]

We shall report on observables which are relevant for an understanding of the bulk properties of nuclear matter under extreme conditions. Previously we have reported[7] on two collective emission patterns of particles *in* the reaction plane: *bounce-off*, which is the sidewards deflection of the spectators, and *side-splash*, which is the transverse momentum transfer between the forward and backward hemispheres of the participants. Recently we reported on a new component of the collective flow in the direction *out* of the reaction plane, which we have called *squeeze-out*.[8] In the present paper we will concentrate on this direction perpendicular to the reaction plane, since that is the only direction where nuclear matter might escape during the whole collision time without being rescattered by either the target or projectile spectators. This provides a window into the hot, dense region of the interacting system. This scenario has been discussed on the basis of hydrodynamics by Scheid *et al.*,[9] being referred to as out-of-plane squeeze-out[10,11,6] and several model calculations have made predictions of this effect.[9,10,12,13] Using data from the Plastic Ball detector[14] we will systematically study the three-dimensional event shape by global variables. We will also study the squeeze-out effect by means of the azimuthal distributions of the particles around the flow axis at mid-rapidity, and, finally, show the rapidity dependence of the effect.

B. Sphericity analysis

The kinetic energy[15] flow tensor

$$F_{ij} = \sum_{\nu} p_i(\nu) p_j(\nu)/2m(\nu) \quad (1)$$

is calculated from the momenta of all measured particles in each event. The tensor approximates the event shape by an ellipsoid, whose aspect ratios and whose orientation in momentum space are calculated by diagonalizing the tensor. The first report of finite flow angles by the Plastic Ball group[7] revealed the existence of collective sideward directed flow (side-splash) in relativistic nuclear collisions.[7,16] The presence of well defined finite flow angles in the data indicates that in those events a reaction plane exists that is defined by the flow axis and the beam axis. Particle tracks from different events can be combined by rotating the events around the beam axis so that

their individual reaction planes line up. Triple differential cross sections of all the events relative to the reaction plane may then be obtained.[10] There has been some evidence (though with large quoted errors) of squeeze-out from previous sphericity analyses.[17,18]

C. Transverse momentum analysis

Based on the observation that the reaction plane can be determined from the collective transverse momentum transfer,[19,20] Danielewicz and Odyniec proposed a more differential way to analyze the momentum contained in directed sidewards emission.[20] They proposed presenting the data in terms of the mean transverse momentum per nucleon in the reaction plane, $\langle p_x/A \rangle$, as a function of the rapidity. Studying the momentum transfer as a function of rapidity permits one to distinguish between participant and spectator contributions and to exclude regions with large detector bias.

In the transverse momentum analysis the reaction plane is determined by the vector $\mathbf{Q}$ calculated for each event from the transverse momentum components $\mathbf{p}_\perp$ of all the particles observed in the forward and backward hemispheres in the center of mass

$$\mathbf{Q} = \sum_i \mathbf{p}_{\perp i}^{forw} - \sum_i \mathbf{p}_{\perp i}^{back} . \quad (2)$$

Each event can be rotated around the beam axis so that $\mathbf{Q}$ defines the x axis of a new coordinate system. It has been shown[21] that the reaction plane determined this way is strongly correlated event by event with the one determined by the sphericity method.

D. Azimuthal distributions

The sphericity and transverse momentum analyses have so far been the most commonly applied methods for analyzing data in terms of collective flow variables. However, both methods, as well as multi-particle correlation functions,[22,23] do not exhaust all the information that is in principle available from 4π spectrometers, and have usually been used to investigate collective phenomena appearing *in* the reaction plane. One would expect that strong collective phenomena perpendicular to the reaction plane take place particularly at mid-rapidity as a result of the large compression effects achieved in the overlap zone. Similar criticisms have been expressed also by Welke *et al.*,[24] who proposed analyzing the azimuthal distributions of particles with respect to the reaction plane as a useful probe of the EOS. A first indication of such an out-of-plane peak in the azimuthal distribution of particles around the beam axis at mid-rapidity was reported by the Diogène group for Ne-induced reactions.[25,26]

In our previous work[8] on squeeze-out we employed an analysis which used the transverse momentum method to determine the reaction plane and the sphericity method to determine the flow angle in that reaction plane. The symmetry of the reaction plane was imposed on the sphericity tensor by forcing certain of its matrix elements to be zero, thus combining the two methods. This was done because it was thought that the reaction plane was better determined by the transverse momentum method. The results demonstrated that azimuthal distributions around the *flow* axis are much better suited to describe the shape of the event than azimuthal distributions around the *beam* axis. The aspect ratios reported in that paper were derived from such azimuthal distributions measured at mid-rapidity. In addition, it was shown that the azimuthal distribution of the momentum/nucleon of the particles also exhibited the effect, indicating that not only the density of particles is enhanced in the out-of-plane direction, but that these particles are also emitted with a higher average transverse momentum per nucleon.

E. Multiplicity variable

In defining the proton multiplicity, N_p, we attempt to account for all participant protons, including those bound in light composites (d, t, ^{3}He, and ^{4}He). The projectile spectators are largely eliminated by excluding a region in $p_\perp$-rapidity space that is identified by use of low multiplicity, peripheral events. Since the particle multiplicity is related to the impact parameter, we classify the events according to this proton multiplicity. The average multiplicity depends on the target-projectile mass and on the beam energy. To allow meaningful comparisons the multiplicity bins chosen should always correspond to approximately the same range in normalized impact parameter. Our approach has been to divide the multiplicity distribution into bins of constant fractions of the maximum multiplicity. The multiplicity distribution has roughly the same form for all systems and energies: a monotonic decrease with increasing multiplicity with a rather pronounced plateau before the final sharp decrease at the highest multiplicities. Therefore the maximum multiplicity (N_p^{max}) can be defined at the point where the curve drops to one half of the plateau height. The review papers[4,5] contain the values of N_p^{max} for all symmetric systems we have measured. The data accumulated with a minimum bias trigger are then divided into 5 bins, 4 equal width bins between 0 and maximum multiplicity and one bin with multiplicities larger than N_p^{max}. These multiplicity bins are labelled MUL1, MUL2, MUL3, MUL4, and MUL5 and range from peripheral collisions with few observed charges to central collisions with very high multiplicities. When more detailed information on the multiplicity dependence is needed, each MUL bin is further divided into five more bins. Although the spectators are not counted in the determination of the N_p variable, all particles are included in the analysis presented below. All the data to be presented have been obtained with a minimum bias trigger.

F. Outline

In this paper we will first compare the sphericity and transverse momentum methods for determining the reac-

tion plane and conclude that they are equally accurate. Then, based on the sphericity method we will demonstrate the effect of out-of-plane squeeze-out, and quantify it with the squeeze-out ratio derived from the two smaller semi-axes of the ellipsoid. The dependence of this ratio on multiplicity, target-projectile mass, and beam energy will be systematically presented. Next we will present azimuthal distributions of the particles around the flow axis at mid-rapidity. Finally we will develop another analysis method based on the transverse momentum method. However, instead of presenting the first moment of $p_\perp$ in the reaction plane as a function of rapidity, we will calculate the ratio of the second moments of $p_\perp$ in the out-of-plane and in-plane directions as a function of rapidity.

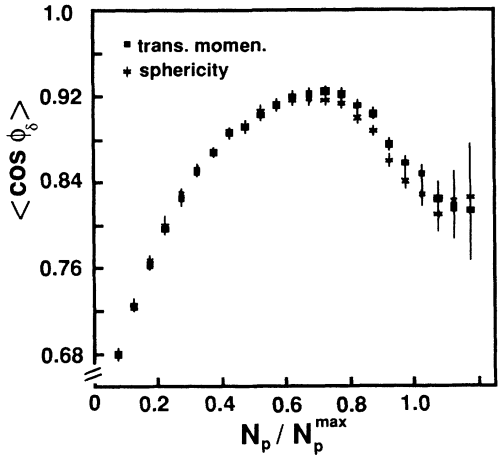

FIG. 1. The mean cosine of the azimuthal difference between the estimated and the true reaction planes calculated from the correlation of the reaction planes of two subevents. Both the sphericity method and the transverse momentum method are shown for the system Au+Au at 400 MeV/nucleon as a function of normalized multiplicity.

II. REACTION PLANE DETERMINATION

The determination of the reaction plane is the first step in the global analysis of the events. The true reaction plane can only be approximated due to the finite multiplicity of charged particles in each event. The two methods which have been used for determining the reaction plane are the sphericity[15] method and the transverse momentum method.[20] We have investigated both methods in order to get an estimate of the achievable accuracy. We have calculated both $\langle |\phi_\delta| \rangle$ and $\langle \cos \phi_\delta \rangle$, where ϕ_δ is the angle between the estimated and the true plane. These quantities are estimated[20] by randomly subdividing the full event into two subevents each containing one half of the particles. The reaction planes determined for the two subevents will in general not coincide due to the nonzero dispersion. The mean of the distribution of the absolute value of one half the azimuthal angle between the two subevent reaction planes is an estimate for $\langle |\phi_\delta| \rangle$, and the mean of the cosine of one half the angle is an estimate for $\langle \cos \phi_\delta \rangle$. The reduction by the factor of one half has two sources: a factor $1/\sqrt{2}$ comes from the change from the two sampling variables to one, and another factor of $1/\sqrt{2}$ from the increase in multiplicity for the whole event.

Figure 1 shows $\langle \cos \phi_\delta \rangle$ for both the sphericity and the transverse momentum methods as a function of the normalized multiplicity. The error bars are derived by assuming that the only contribution is the statistical uncertainty in the individual data points of the distribution. The factors are in the numerical range of approximately 0.7 to 0.9, increasing with the number of particles and then decreasing as the event becomes more spherical. A higher value implies a better determination of the reaction plane since the factor will have a value of 1.0 in the limiting case of zero dispersion. Figure 1 shows that the two methods generate factors which are within one standard deviation at low to medium multiplicity. At high multiplicity, the transverse momentum method gives a slightly better determination of the reaction plane. The overall similarity of the factors determined by the two different methods indicates, however, that the two methods generate very similar dispersion for the reaction plane and that the results therefore differ from the true reaction plane by about the same amount. Thus both the sphericity and the transverse momentum methods are equally well suited to determine the reaction plane in this system. Moreover, for our data, no conclusive evidence was found for a systematic decrease in the reaction plane dispersion by excluding mid-rapidity particles as done previously.[8,20,27] The factors generated by applying different mid-rapidity cuts are all within two standard deviations of the factors generated by including all the particles. A mid-rapidity cut was therefore not used in any of the following analyses.

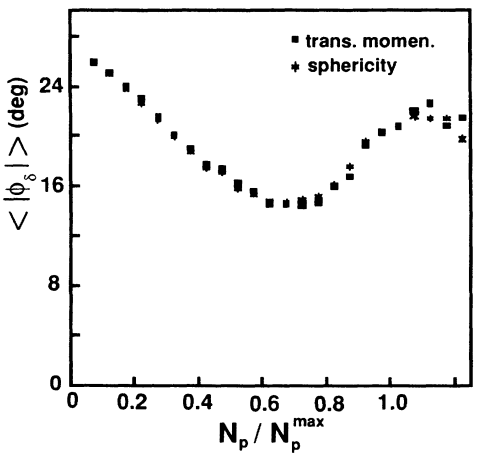

FIG. 2. The mean value of the absolute azimuthal difference between the estimated and the true reaction planes for the system Au+Au at 400 MeV/nucleon for the sphericity method and the transverse momentum method as a function of normalized multiplicity.

Although the $\langle \cos \phi_\delta \rangle$ factor is also normally used to correct $\langle p_x \rangle$ values for the reaction plane dispersion, this paper will be concerned with ratios of out-of-plane to in-plane quantities, where the corrections partially cancel out and are quite complicated. Therefore, we have not made any such corrections to the data to be presented, but assume that when acceptance filtered simulations are compared to our data, the sphericity method will be used in the same way to determine the reaction plane.

In Fig. 2 we also show $\langle |\phi_\delta| \rangle$ as a function of normalized multiplicity. The angles are astonishingly small, a fact that makes the concept of global analysis at these multiplicities so successful.

III. SPHERICITY METHOD

A. Method

The sphericity method reduces the information contained in the 4-momenta of all the measured charged particles to a set of six variables, i.e., the three eigenvalues describing the shape of an ellipsoid (see Fig. 3) and a set of three Euler angles describing the absolute orientation of the ellipsoid. The plane spanned by the beam axis and by the eigenvector $\mathbf{e}_3$ is identified as the reaction plane. ($\mathbf{e}_j$ is the eigenvector generated by the eigenvalue λ_j with $\lambda_1 \leq \lambda_2 \leq \lambda_3$.) Since any azimuthal dependence of parameters is only relevant with respect to the reaction plane, the azimuth of $\mathbf{e}_3$ is chosen to be 0° for each event. This transformation reduces the three Euler angles to a set of two angles which unambiguously characterizes the orientation of the ellipsoid. The two angles are chosen to be the polar angle of $\mathbf{e}_3$ identified as the flow angle, θ_{flow}, and the angle ψ_{sq} referred to as the squeeze angle. The squeeze angle is used to describe the orientation of $\mathbf{e}_1$ and $\mathbf{e}_2$ around the flow axis relative to the reaction plane. Precisely, ψ_{sq} is chosen to be the angle by which $\mathbf{e}_2$ needs to be rotated around the $\mathbf{e}_3$ axis in order to be transformed into the reaction plane (see Fig. 3).

Figure 4 shows a distribution of the squeeze angle in the Au+Au system at 400 MeV/nucleon for semi-central collisions (MUL3). The maximum at 90° shows that there is strong alignment of $\mathbf{e}_2$ in the out-of-plane direction, i.e., the kinetic energy flow around the flow axis appears predominantly *perpendicular* to the reaction plane. The squeeze angle must be symmetric about either 0° or 90° on the average, and in the absence of any preferred emission, or in other words, in the case of a rotational symmetric *spheroid*, the angular distribution would be flat. This experimental observation of a *strong peaking* at 90° with respect to the reaction plane confirms the first results[8] on out-of-plane squeeze-out.

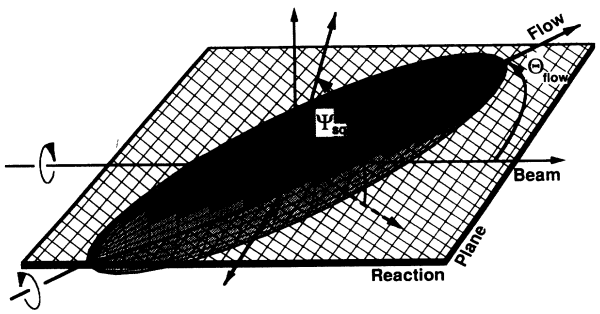

FIG. 3. A perspective view of a tri-axial ellipsoid. The major flow axis and the beam axis define the polar flow angle, θ_{flow}, and the reaction plane. The squeeze angle, ψ_{sq}, is defined as the azimuthal angle around the flow axis of the medium axis of the ellipsoid relative to the reaction plane.

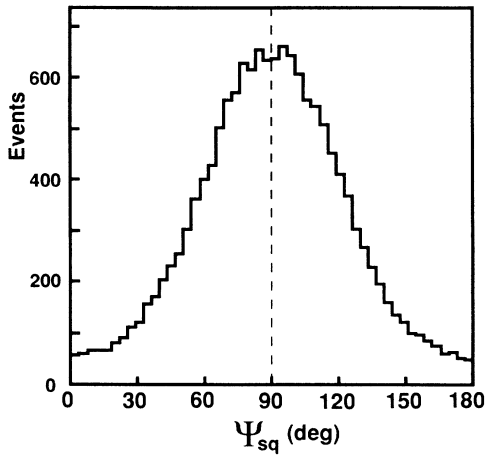

FIG. 4. The distribution of the squeeze angle for the system Au+Au at 400 MeV/nucleon for the multiplicity bin MUL3 as determined by the sphericity method.

Global analysis using the sphericity method has the advantage that the event shapes are reduced to a small number of parameters which can easily display trends in the data. However, it must be remembered that distortions from the Plastic Ball acceptance affect the results and that all the particles (including the spectators) are used in the analysis. It has also been pointed out how finite number effects can distort the results at low multiplicities.[28]

Quantitatively, the in-plane flow is determined for each event by forming the ellipse spanned by $\mathbf{e}_1$ and $\mathbf{e}_2$ and by calculating its intersection point with the reaction plane as shown in Fig. 5. The resulting length between the center of the ellipse and the intersection point is a quantity characterizing the in-plane flow. The out-of-plane flow is determined similarly but using the intersection between the ellipse and the perpendicular to the reaction plane through the origin (see Fig. 5). The mean of the ratio of the out-of-plane to in-plane values is given the name *sphericity squeeze-out ratio*, and the symbol R_λ. The quoted uncertainty in R_λ is calculated by assuming that only the statistical uncertainty in the number of events contributes to the uncertainty of the mean. Whereas the ratio of the lengths of the medium eigenvector to the smallest eigenvector is always greater than one by definition, the sphericity squeeze-out ratio is not restricted to being greater than one.

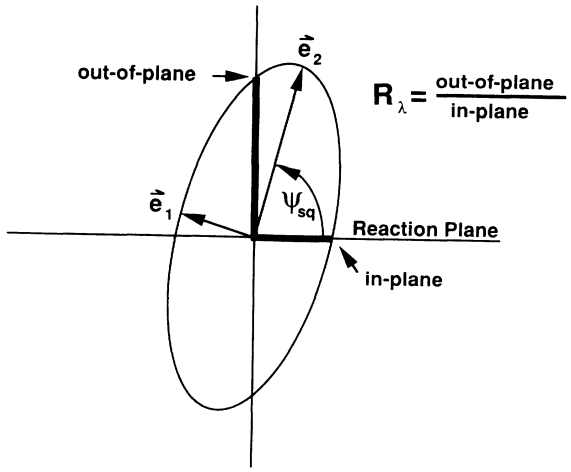

FIG. 5. The plane perpendicular to the flow axis through the origin, showing how R_λ is calculated from the two smaller eigenvalues and the reaction plane.

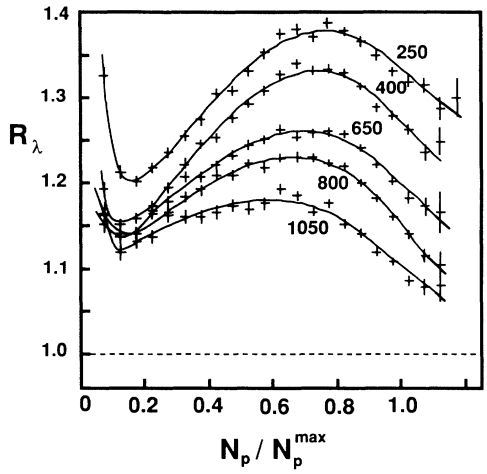

FIG. 7. The sphericity squeeze-out ratio for the Au+Au system at 250 MeV/nucleon and higher energies shown as a function of the normalized multiplicity.

B. Multiplicity dependence

Figures 6 and 7 show the multiplicity dependence of the squeeze-out ratio, R_λ, in the Au+Au system at different beam energies. The steep increase of R_λ at very low multiplicities is due to fluctuations. This is simply because the mean of the ratios of two random numbers is usually greater than one. However, peaks at medium multiplicities are well defined and the contribution of fluctuations is estimated to be small by extrapolating the steeply decreasing left-hand side of the curves to the region under the peaks. The highest value of R_λ is reached at the beam energy of 250 MeV/nucleon and the squeeze-out ratios at beam energies above and below this energy are plotted in two separate graphs. In the two graphs, the peak shifts from central to semi-central collisions as the beam energy increases.

A similar behavior of R_λ is found for the Nb+Nb system shown in Figs. 8 and 9. The maximum in R_λ is now shifted towards a higher beam energy approaching 400 MeV/nucleon. The lowest beam energy of 150 MeV/nucleon shows that R_λ does not decrease even for the most central collisions at this energy, which is similar to the Au+Au system. One wonders if the flattening of the curves at low beam energies is due to a transition to an oblate shape. However, the sphericity versus coplanarity plot[29,30] shows more dispersion in the event shapes at the lower beam energies, but no clear transition to oblate shapes. The multiplicity dependence of R_λ in the Ca+Ca system is shown in Fig. 10. R_λ shows a very broad plateau from semi-central collisions to the most central collisions at both energies measured. Here, the fluctuations as indicated by the left-hand side

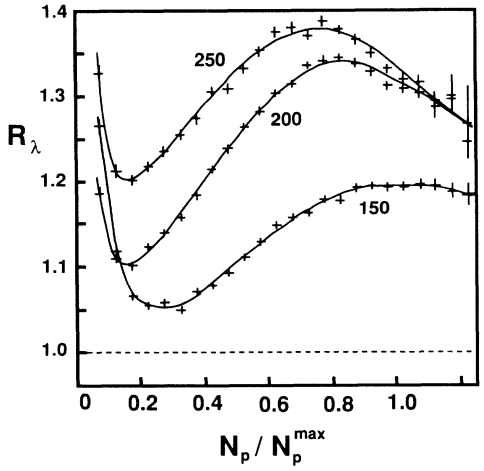

FIG. 6. The sphericity squeeze-out ratio for the Au+Au system at 250 MeV/nucleon and lower energies shown as a function of the normalized multiplicity.

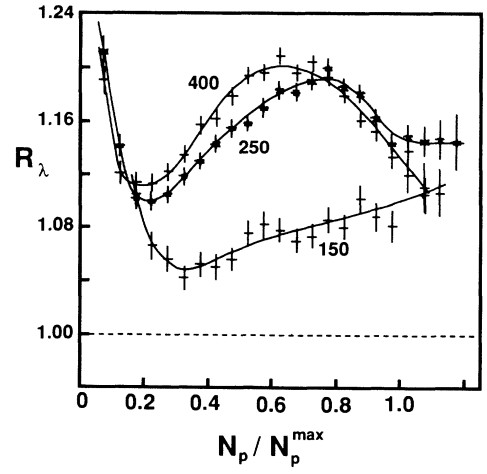

FIG. 8. The sphericity squeeze-out ratio for the Nb+Nb system at 400 MeV/nucleon and lower energies shown as a function of the normalized multiplicity.

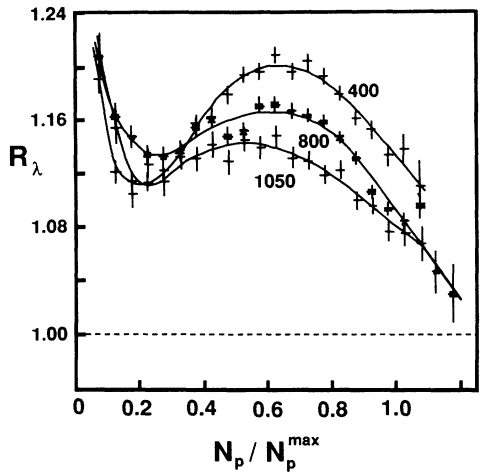

FIG. 9. The sphericity squeeze-out ratio for the Nb+Nb system at 400 MeV/nucleon and higher energies shown as a function of the normalized multiplicity. The 650 MeV/nucleon data, which are not plotted, lie just above the 800 MeV/nucleon points.

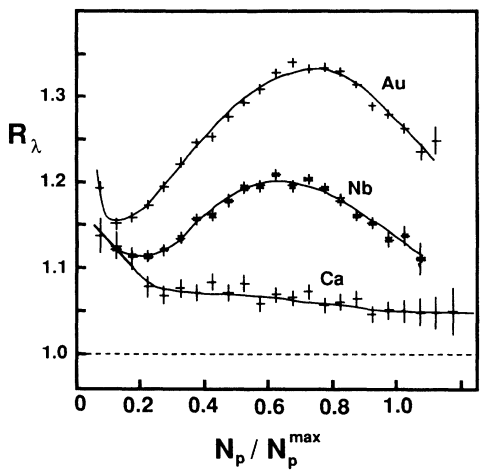

FIG. 11. The sphericity squeeze-out ratio for the three systems Au+Au, Nb+Nb and Ca+Ca at the beam energy of 400 MeV/nucleon shown as a function of the normalized multiplicity.

of the curves, are apparently not negligible. In comparing with the previously reported side splash effect, it should be noted that, although in most cases for all three systems R_λ peaks at mid-multiplicity, as does the *flow* effect,[31,27] the behavior is quite different from that for the flow *angles*,[21] which increase continuously with increasing multiplicity.

C. Mass and energy dependence

Figure 11 shows R_λ for the systems Ca+Ca, Nb+Nb, and Au+Au at 400 MeV/nucleon as a function of multiplicity. The plateau in the distribution of the Ca+Ca system is found at a value of about 1.07. The Nb+Nb system, however, has a distinctive peak at a value of approximately 1.20, whereas the peak in the Au+Au is found at approximately 1.33. Figure 11 shows a clear increase of R_λ with increasing mass at comparable normalized impact parameter.

The energy dependence of R_λ shown in Fig. 12 was obtained by taking the peak values of R_λ and their error bars above the fluctuation region, and plotting them as a function of beam energy for the three systems measured. The two heavier mass systems clearly show a steep increase in R_λ from the lowest energy of 150 MeV/nucleon to the maximum R_λ at around 250 MeV/nucleon with a subsequent smooth decrease with increasing energy. The lighter system Ca+Ca does not show any significant energy dependence at the two energies measured. For the heavier systems this beam energy dependence of R_λ is quite different from the side-splash effect reported earlier,[31,27] where the *flow* rises gradually up to about 600 MeV/nucleon and then levels off.

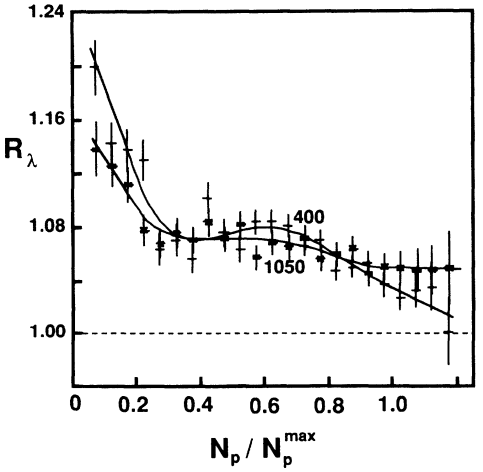

FIG. 10. The sphericity squeeze-out ratio for the Ca+Ca system at the two energies measured shown as a function of the normalized multiplicity.

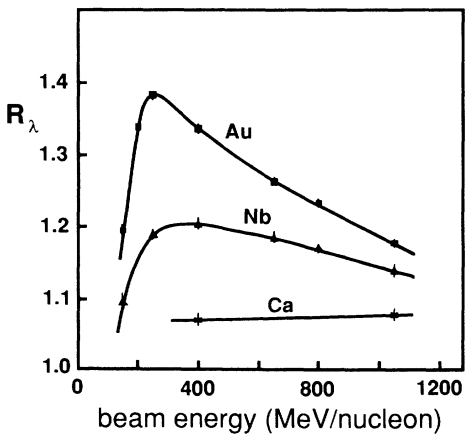

FIG. 12. The peak values of the sphericity squeeze-out ratio in the three systems Au+Au, Nb+Nb and Ca+Ca. The values are shown for all the beam energies at which the systems were measured. The curves are just to guide the eye.

IV. AZIMUTHAL DISTRIBUTIONS

Now that the flow axis has been determined by the sphericity method, we may look at the azimuthal distributions of various particles around the flow axis[8] as another way to investigate the preferred emission direction with respect to the reaction plane. Autocorrelations for each particle have been removed by diagonalizing the sphericity matrix of all the other particles. Figure 13 shows the yield of particles as a function of the *azimuthal angle* around the *flow* axis, called ψ, and the momentum *along* the flow axis. The mountain peak is due to projectile spectators in the reaction plane and the two ridges at $\pm 90°$ are a very graphic representation of the squeeze-out process which we are studying. To avoid the spectator effects we set a window, as previously,[8] on the momentum component along the flow axis centered at mid-rapidity and equal to $\pm 10\%$ of the momentum of the beam. We will extend our previous investigations of these azimuthal distributions,[8,32] by studying further the dependence on projectile-target mass and beam energy, as well as on the emitted particle species.

Figure 14 shows the azimuthal distributions for the multiplicity bin MUL3 for the Au+Au system at all the energies measured. These distributions show both a four-fold symmetry from the shape of the ellipsoids and a two-fold symmetry from two effects. The first effect is caused by the acceptance of the Plastic Ball even though the chosen narrow window minimizes spectator contributions. Although the Plastic Ball acceptance is symmetric around the beam axis it is not symmetric about the flow axis. The rotation by the flow angle converts the detector acceptance asymmetry between the backward and forward hemispheres into an asymmetry between 0° and 180° in the azimuthal distributions. This is because the window used for plotting the data is perpendicular to the flow axis, not the beam axis, and therefore, for finite flow angles the particles near 0° are backwards of mid-rapidity, and the particles near 180° are forwards of mid-rapidity. Target absorption leads to depletion at an azimuth of 0° whereas punch-through particles are lost in the forward direction which is at an azimuth of 180° in the rotated system. The second effect is caused by the window not being centered exactly at mid-rapidity due to slight calibration errors, and also not perpendicular to the local flow axis for the particles in the window because it is set to be perpendicular to the flow axis for the entire event. These differences together can cause the side-splash to falsely contribute to the azimuthal distributions in the window. In Fig. 14 the shift of the depletion from 0° at low energies to 180° at high energies reflects the contributions of these two effects. These effects apparently result in a contribution to the distributions closely proportional to $\cos(\psi)$, whereas the true azimuthal correlations must result in a contribution to the distributions proportional to $\cos(2\psi)$. The smooth curves shown in Fig. 14 which are superimposed on the experimentally measured azimuthal distributions are an expansion of the form

$$N(\psi) \propto 1 + S_1 \cos(\psi) + S_2 \cos(2\psi) \, . \tag{3}$$

As can be seen, this two parameter expansion gives an

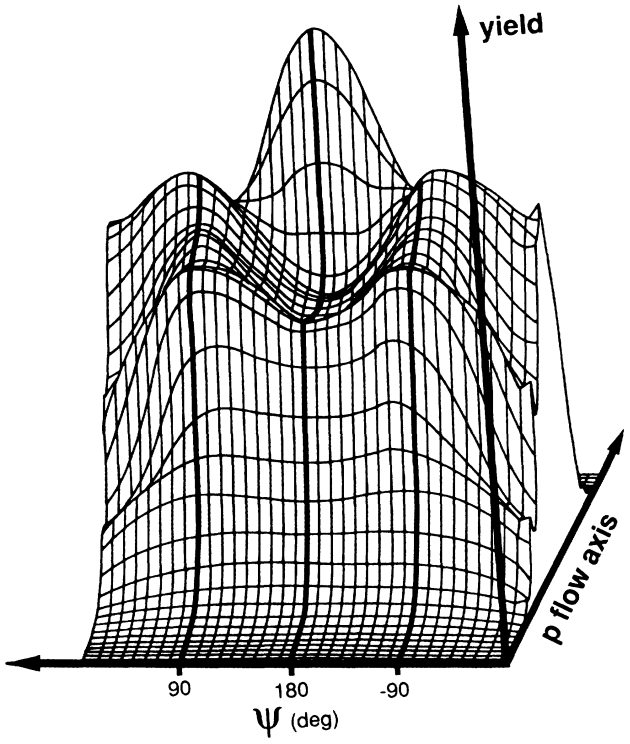

FIG. 13. Isometric projection of the yield of particles for 400 MeV/nucleon Au+Au as a function of the momentum along the flow axis and the azimuthal angle around the flow axis.

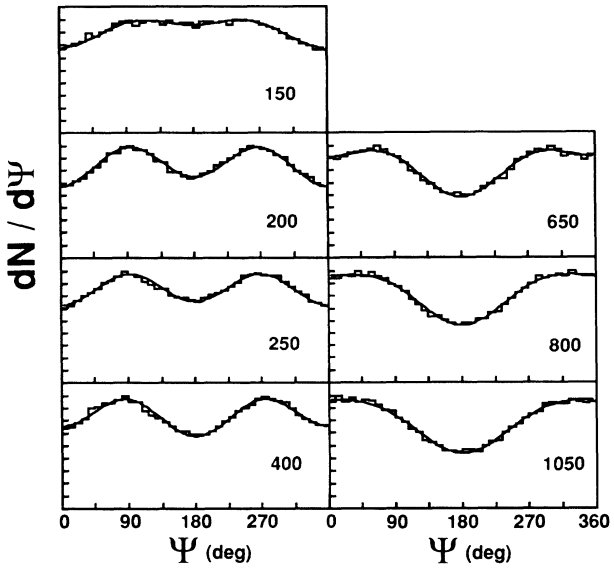

FIG. 14. Azimuthal distributions around the flow axis in the window near mid-rapidity for multiplicity bin MUL3 for Au+Au at the indicated beam energies in MeV/nucleon. The ordinate is linear starting at zero. The smooth curves are fits with $\cos(2\psi)$ and $\cos(\psi)$ terms.

excellent approximation to all the measured azimuthal distributions. It appears that the $\cos(\psi)$ term nicely accounts for the two effects and allows us to extract the coefficient of the $\cos(2\psi)$ term in order to quantify the squeeze-out effect.

The *number squeeze-out ratio* is defined as the number of particles at mid-rapidity emitted perpendicular to the reaction plane divided by the number of particles emitted in the reaction plane, and is given by

$$R_N = \frac{N(90°) + N(-90°)}{N(0°) + N(180°)} = \frac{1 - S_2}{1 + S_2} . \quad (4)$$

The values of R_N are shown in Fig. 15 for the Au+Au, Nb+Nb and Ca+Ca systems for the MUL3 bin at all the energies measured. R_N is significantly greater than one for all the data except the lowest energy Nb point. The Au point at 200 MeV/nucleon is high because intermediate mass fragments were measured in this experiment[33] and included in the analysis. It is shown below in Fig. 19 that $Z=2$ fragments exhibit more squeeze-out than protons. It is ironic that just in this case, 200 MeV/nucleon Au+Au, where the squeeze-out effect is largest, our originally published[33] azimuthal distributions did not show the effect. That is because the distributions were around the beam axis, not the flow axis, and although there was a window near mid-rapidity, it was too wide.

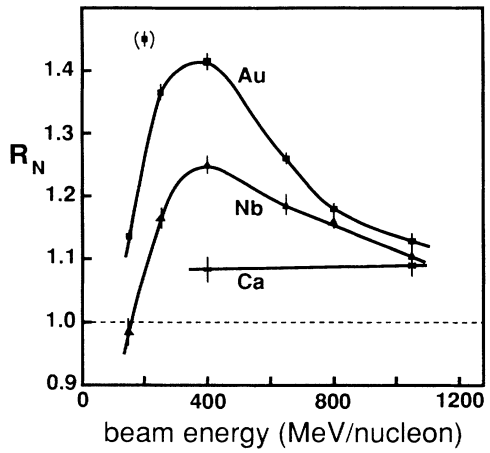

FIG. 15. The number squeeze-out ratio for data in the multiplicity bin MUL3 for the three systems Au+Au, Nb+Nb and Ca+Ca. The values are shown for all the beam energies at which the systems were measured. The Au point at 200 MeV/nucleon, which is in parentheses, includes intermediate mass fragments. The curves are just to guide the eye.

In general, the energy and target-projectile mass dependence from the azimuthal distributions of particles which is shown in Fig. 15 substantiates the behavior obtained from the global parameters shown in Fig. 12. It should be noted that while the data in Fig. 12 are from

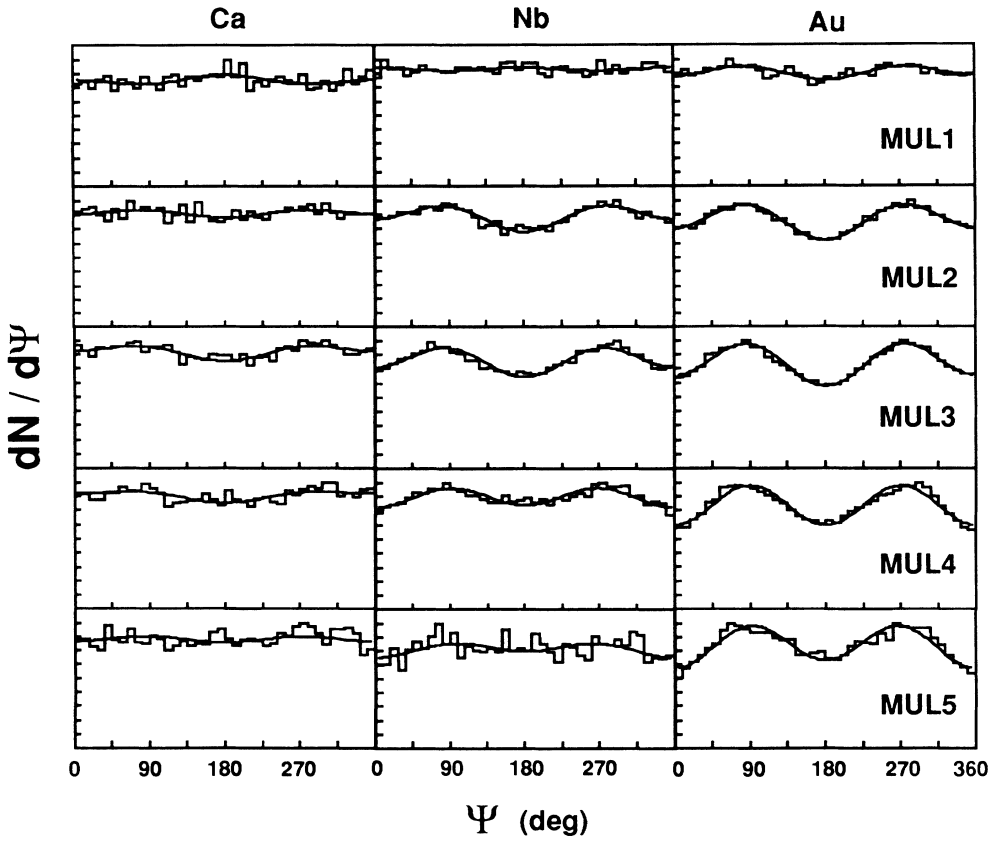

FIG. 16. Azimuthal distributions around the flow axis in the window near mid-rapidity for the five multiplicity bins and the three target-projectile combinations at 400 MeV/nucleon beam energy. The ordinate is linear starting at zero. The smooth curves are fits with $\cos(2\psi)$ and $\cos(\psi)$ terms.

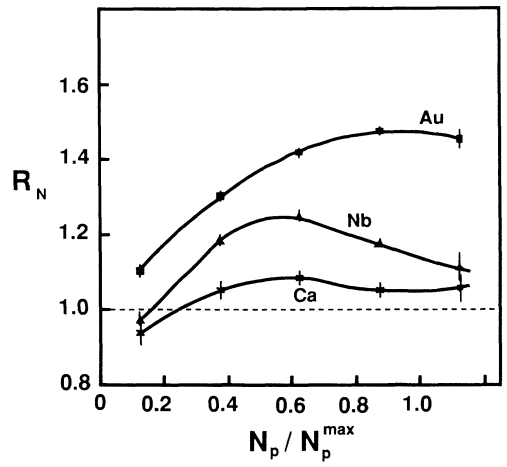

FIG. 17. The number squeeze-out ratio for the three systems Au+Au, Nb+Nb and Ca+Ca at the beam energy of 400 MeV/nucleon shown as a function of the normalized multiplicity. The curves are just to guide the eye.

the peak values as a function of multiplicity, the data in Fig. 15 are for MUL3. The mass dependence is similar to that in our preliminary work,[32] but the values of R_N are smaller. There are several differences between the method described in this section and the one we have used before.[8,32] In our previous work the reaction plane was determined by the transverse momentum method and the flow angle from the sphericity method. Here, both are determined by the sphericity method. Previously, the particles were weighted by the momentum[8] or the transverse energy[32] to increase the effect. (The description of Fig. 4 in Ref. 8 was not quite correct. The filled circles give the aspect ratio, not of the particles, but of the particles weighted by their momentum per nucleon. The momentum per nucleon was plotted correctly in the lower curve.) Finally, in this analysis we have fit the complete azimuthal distributions with a functional form which accounts to first order for the lack of symmetry between forward and backward hemispheres.

Figure 16 shows the azimuthal distribution for the three systems Au+Au, Nb+Nb and Ca+Ca at 400 MeV/nucleon for the five standard multiplicity bins. Figure 17 displays the corresponding values of R_N for these three systems. Note that for the Nb+Nb and Ca+Ca systems for the most peripheral collisions the particles tend to be emitted in the reaction plane. At this energy the R_N values in the MUL3 bins are at, or near, the peak values.

We have shown that composite particles show more pronounced flow effects than protons alone.[33] Therefore

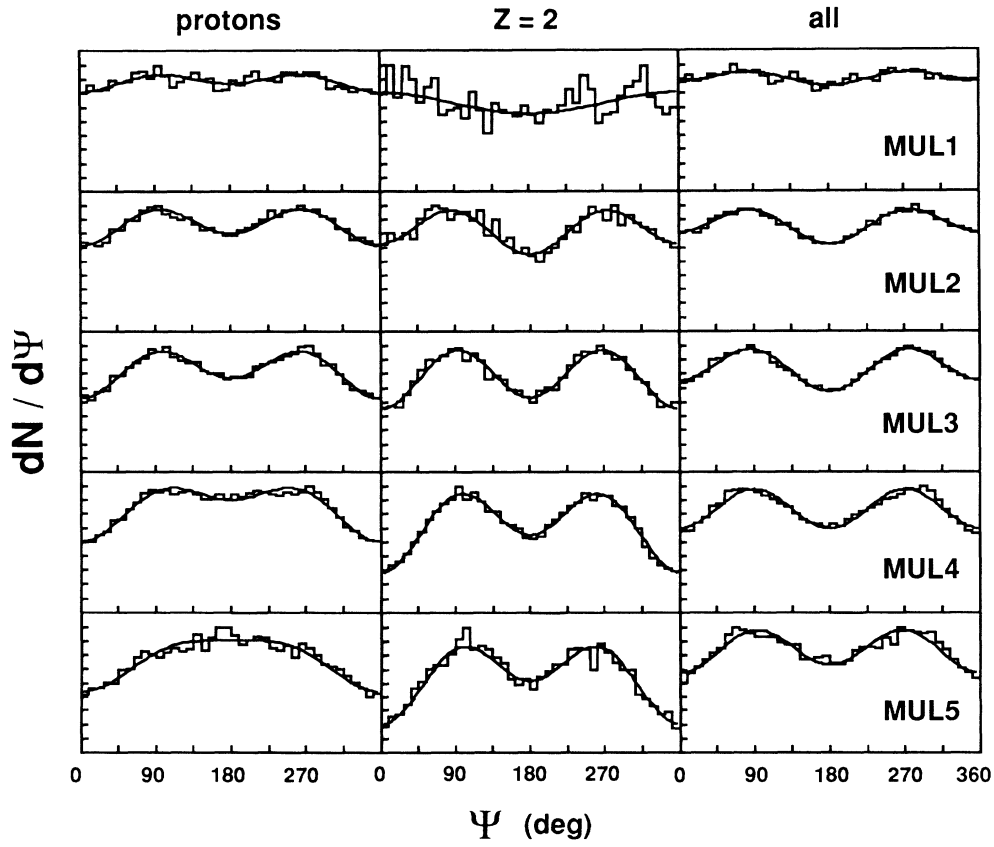

FIG. 18. Azimuthal distributions around the flow axis in the window near mid-rapidity for the five multiplicity bins for 400 MeV/nucleon Au+Au. The data are shown separately for protons, Z=2 particles, and all the particles together. The ordinate is linear starting at zero. The smooth curves are fits with $\cos(2\psi)$ and $\cos(\psi)$ terms.

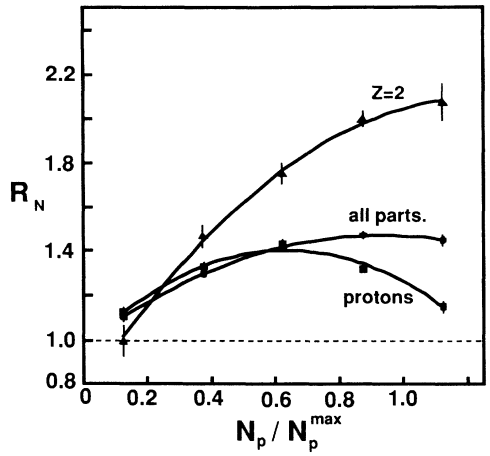

FIG. 19. The number squeeze-out ratio for protons, Z=2 particles, and all the particles, for 400 MeV/nucleon Au+Au shown as a function of the normalized multiplicity. The curves are just to guide the eye.

it is interesting to investigate the dependence of the azimuthal distributions on particle species. This is shown in Fig. 18 for protons, Z=2 particles, and all the particles in the Au+Au system at 400 MeV/nucleon for the five standard multiplicity bins. The corresponding R_N values are displayed in Fig. 19. Again the Z=2 particles show a much stronger effect than the protons. In addition the effect for Z=2 particles continues to rise to high multiplicities.

V. TRANSVERSE MOMENTUM METHOD

A. Method

Another completely independent method was used to investigate the rapidity dependence of the squeeze-out effect. First, each event is rotated so that the reaction plane determined by the transverse momentum method determines the zero of the azimuthal angle around the beam axis. In this new method, the flow in-plane and out-of-plane are determined from the second moments of the transverse momentum components in plane, $\langle (p_x - \langle p_x \rangle)^2 \rangle$, and out of plane, $\langle (p_y - \langle p_y \rangle)^2 \rangle$. We define the $p_\perp$ *squeeze-out ratio*, $R_p(y)$, as the ratio of the moments out-of-plane to in-plane. By expanding and dropping the cross terms, it can be written as

$$R_p(y) = \frac{\langle p_y^2 \rangle - \langle p_y \rangle^2}{\langle p_x^2 \rangle - \langle p_x \rangle^2} \,. \tag{5}$$

The term $\langle p_y \rangle$ is zero on the average by symmetry with respect to the reaction plane but is kept because of its contribution to the dispersion of the ratio. In effect, the numerator is the width of the transverse momentum distribution in the out-of-plane direction, and the denominator is the width of the in-plane distribution corrected for the mean p_x values caused by the side-splash.

B. Rapidity dependence

The rapidity dependence of $R_p(y)$ in the system Au+Au at 400 MeV/nucleon is shown in Fig. 20 for the standard five multiplicity bins. The figure shows the qualitative behavior of an approximately constant squeeze-out at all rapidities, confirming our previous observations based on the azimuthal distributions of particles.[8] The multiplicity dependence of the plateau values, when compared to the values derived by the sphericity method and shown already in Fig. 11, are approximately the same, but fall off faster at high multiplicities. This can be understood since at finite flow angles a *spheroid* would have $R_p(y)$ values less than one in this method because the dispersion in the out-of-plane direction is measured perpendicular to the symmetry plane, while the dispersion in-plane is bigger because it is measured perpendicular to the beam axis, not the flow axis. Also, where there are spectator fragments, they decrease the ratio both by increasing the dispersion in the in-plane direction and by decreasing the mean p_x value. It should be noted that in this transverse momentum method the projection of the squeeze-out effect on to the beam axis causes some smearing of the squeeze-out effect. However, the advantage is that it is the natural extension of the

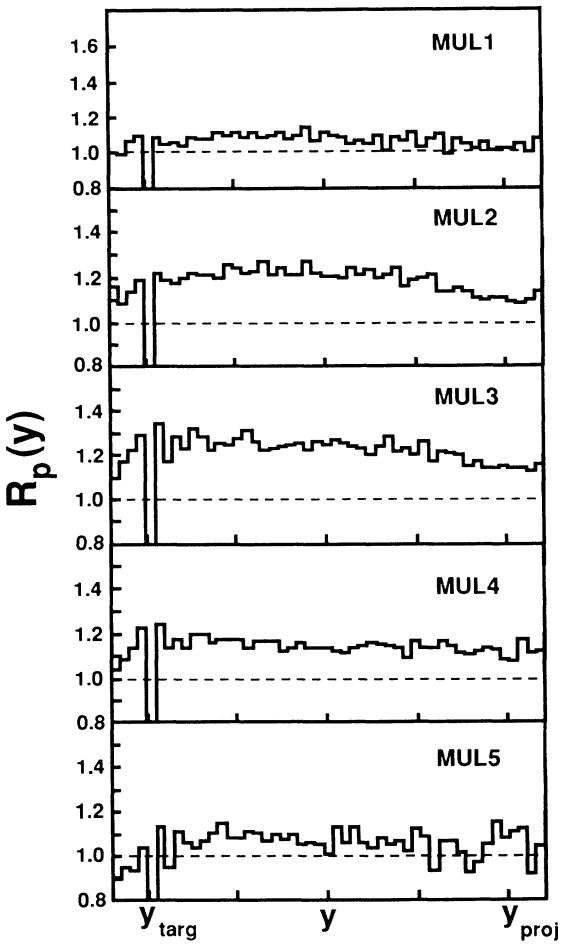

FIG. 20. The $p_\perp$ squeeze-out ratio as a function of rapidity for 400 Mev/nucleon Au+Au for the five multiplicity bins.

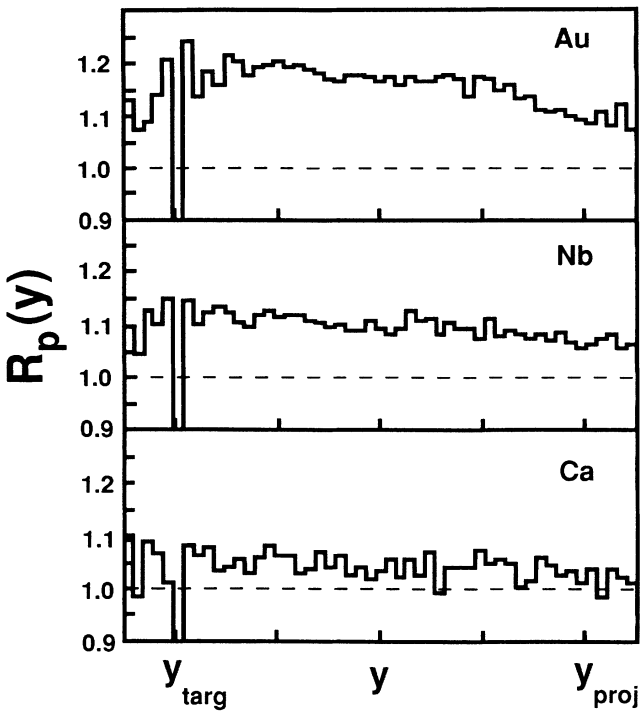

FIG. 21. The $p_\perp$ squeeze-out ratio as a function of rapidity for 400 MeV/nucleon Au+Au, Nb+Nb, and Ca+Ca.

method of plotting $\langle p_\perp \rangle$ versus y, and is independent of the sphericity method.

In Fig. 21 the data for all the multiplicity bins have been combined and shown for the three target-projectile combinations. The dependence of the plateau values on target-projectile mass is slightly less than found by the sphericity method and shown already in Fig. 11. This is because for the heavier targets the flow angles are larger and this lowers the ratio as described above with the example of a spheroid.

VI. CONCLUSIONS

The sphericity and transverse momentum methods have about equal accuracy in determining the reaction plane. Most importantly, the sphericity method shows a strong alignment of the medium length eigenvector in the out-of-plane direction. The sphericity squeeze-out ratio, which quantifies this effect, shows a maximum for semi-central collisions and increases with target-projectile mass. The effect peaks at surprisingly low beam energy, in contrast to the previously reported side-splash effect. This is disturbing because both effects describe the shape of the flow ellipsoid and one would think they would have the same energy dependence. However, the Flow is calculated from the first moment of the p_x distribution but, as we have shown, squeeze-out may be thought of as the ratio of two second moments. As the beam energy increases, thermal smearing effects will wash out an effect in the second moments before the first moment is affected. This is consistent with the experimental observations and may be the explanation for the different energy dependencies. From the azimuthal distribution of the particles at mid-rapidity the number squeeze-out ratio confirms the result from the global sphericity parameters. Finally from the $p_\perp$ squeeze-out ratio it is clear that the effect is not jet-like, but appears at all rapidities.

Thus, a very important piece of information has become available from the observation of the out-of-plane squeeze-out of particles. The fact that the squeeze-out drops at high beam energy may be because the thermal energy is increasing faster than the compressional energy. The reason the heavier fragments exhibit the effect more strongly is probably because at the same thermal energy higher mass fragments have smaller thermal velocity components which disturb the compressional velocity less.[33] Theoretically, for large values of the nuclear viscosity the squeeze-out effect is expected to be damped out, and a peak should not be visible in the azimuthal distributions. Thus, such data will be essential in determining this unknown property of hot nuclear matter. The same sensitivity is also found in microscopic calculations (VUU/BUU, QMD), where the azimuthal distribution depends strongly on the EOS and the effective in-medium cross section, $\sigma_{\rm eff}$, i.e., parameters which enter directly into the coefficients of the viscosity.[34]

Because, in a geometrical picture, squeeze-out particles escape from the hot and dense reaction zone unhindered by surrounding cold target or projectile matter, they provide a clean probe through which one can look directly at the compressed and hot fireball. It will be most interesting in the near future to see whether the successful microscopic models can consistently (using the same EOS and $\sigma_{\rm eff}$) describe the $\langle p_x \rangle / A$, dN/dy, d/p, and squeeze-out ratios. Simultaneous description of all the exclusive experimental observables would be a large step forward in the ultimate goal of relativistic heavy-ion collisions, namely the determination of the bulk properties of nuclear matter.

ACKNOWLEDGEMENTS

We thank Pavel Danielewicz for stimulating conversations, in particular one in which the perpendicular momentum method was devised. For help with Fig. 3 we also thank Craig Tull and Harold Poskanzer. This work was supported in part by the Director, Office of Energy Research, Office of High Energy and Nuclear Physics, Division of Nuclear Physics of the U.S. Department of Energy under Contract DE-AC03-76SF00098.

*Present address: CERN, EP Division, CH-1211 Geneva 23, Switzerland.
[1]N.K. Glendening, Phys. Rev. C **37**, 2733 (1988).
[2]E. Baron, J. Cooperstein, and S. Kahana, Phys. Rev. Lett. **55**, 126 (1985).
[3]J.R. Wilson and H.A. Bethe, Astrophys. J. **295**, 14 (1985).
[4]K.-H. Kampert, J. Phys. G **15**, 691 (1989).
[5]H.H. Gutbrod, A.M. Poskanzer, and H.G. Ritter, Rep. Prog. Phys. **52**, 1267 (1989).
[6]H. Stöcker and W. Greiner, Phys. Reports **137**, 277 (1986).
[7]H.Å. Gustafsson, H.H. Gutbrod, B. Kolb, H. Löhner, B. Ludewigt, A.M. Poskanzer, T. Renner, H. Riedesel, H.G. Ritter, A. Warwick, F. Weik, and H. Wieman, Phys. Rev. Lett. **52**, 1590 (1984).
[8]H.H. Gutbrod, K.H. Kampert, B. Kolb, A.M. Poskanzer, H.G. Ritter, and H.R. Schmidt, Phys. Lett. B **216**, 267 (1989).
[9]W. Scheid, H. Müller, and W. Greiner, Phys. Rev. Lett. **32**, 741 (1974).
[10]H. Stöcker, L.P. Csernai, G. Graebner, G. Buchwald, H. Kruse, R.Y. Cusson, J.A. Maruhn, and W. Greiner, Phys. Rev. C **25**, 1873 (1982).
[11]G. Buchwald, G. Graebner, J. Theis, J. Maruhn, W. Greiner, H. Stöcker, K. Frankel, and M. Gyulassy, Phys. Rev. C **28**, 2349 (1983).
[12]M.I. Sobel, P.J. Siemens, and H.A. Bethe, Nucl. Phys. **A251**, 502 (1975).
[13]J. Kapusta and D. Strottman, Phys. Lett. **106B**, 33 (1981).
[14]A. Baden, H.H. Gutbrod, H. Löhner, M.R. Maier, A.M. Poskanzer, T. Renner, H. Riedesel, H.G. Ritter, H. Spieler, A. Warwick, F. Weik, and H. Wieman, Nucl. Instrum. Methods **203**, 189 (1982).
[15]M. Gyulassy, K.A. Frankel, and H. Stöcker, Phys. Lett. **110B**, 185 (1982).
[16]G. Buchwald, G. Graebner, J. Theis, J. Maruhn, W. Greiner, and H. Stöcker, Phys. Rev. Lett. **52**, 1594 (1984).
[17]P. Danielewicz, in *Proceedings of the Workshop on Gross Properties of Nuclei, Hirschegg*, edited by H. Feldmeier (Technische Hochschule Darmstadt, 1987).
[18]P. Danielewicz, H. Ströbele, G. Odyniec, D. Bangert, R. Bock, R. Brockmann, J.W. Harris, H.G. Pugh, W. Rauch, R.E. Renfordt, A. Sandoval, D. Schall, L.S. Schroeder, and R. Stock, Phys. Rev. C **38**, 120 (1988).
[19]H.Å. Gustafsson, H.H. Gutbrod, B. Kolb, H. Löhner, B. Ludewigt, A.M. Poskanzer, T. Renner, H. Riedesel, H.G. Ritter, T. Siemiarczuk, J. Stepaniak, A. Warwick, and H. Wieman, Z. Physik A **321**, 389 (1985).
[20]P. Danielewicz and G. Odyniec, Phys. Lett. **157B**, 146 (1985).
[21]H.G. Ritter, K.G.R. Doss, H.Å. Gustafsson, H.H. Gutbrod, K.H. Kampert, B. Kolb, H. Löhner, B. Ludewigt, A.M. Poskanzer, A. Warwick, and H. Wieman, Nucl. Phys. **A447**, 3c (1986).
[22]P. Beckmann, H.Å. Gustafsson, H.H. Gutbrod, K.H. Kampert, B. Kolb, H. Löhner, A.M. Poskanzer, H.G. Ritter, H.R. Schmidt, and T. Siemiarczuk, Mod. Phys. Lett. **A2**, 163 (1987).
[23]P. Beckmann, K.G.R. Doss, H.Å. Gustafsson, H.H. Gutbrod, K.H. Kampert, B. Kolb, H. Löhner, A.M. Poskanzer, H.G. Ritter, H.R. Schmidt, T. Siemiarczuk, and H. Wieman, Mod. Phys. Lett. **A2**, 169 (1987).
[24]G.M. Welke, M. Prakash, T.T.S. Kuo, S. DasGupta, and C. Gale, Phys. Rev. C **38**, 2101 (1988).
[25]D. L'Hôte, private communication and talk at Fifth Gull Lake Nuclear Physics Conference, Gull Lake, MI (1988).
[26]J. Gosset, in The Proceedings of the NATO Advanced Study Institute on the Nuclear Equation of State, Peñiscola, Spain, 1989 (to be published).
[27]H.Å. Gustafsson, H.H. Gutbrod, J. Harris, B.V. Jacak, K.-H. Kampert, B. Kolb, A.M. Poskanzer, H.G. Ritter, and H.R. Schmidt, Mod. Phys. Lett. **A3**, 1323 (1988).
[28]P. Danielewicz and M. Gyulassy, Phys. Lett. **129B**, 283 (1983).
[29]S.L. Wu and G. Zoberning, Z. Phys. C **2**, 107 (1979).
[30]G. Fai and J. Randrup, Nucl. Phys. **A404**, 551 (1983).
[31]K.G.R. Doss, H.Å. Gustafsson, H.H. Gutbrod, K.H. Kampert, B. Kolb, H. Löhner, B. Ludewigt, A.M. Poskanzer, H.G. Ritter, H.R. Schmidt, and H. Wieman, Phys. Rev. Lett. **57**, 302 (1986).
[32]H.R. Schmidt, H.H. Gutbrod, K.H. Kampert, B. Kolb, A.M. Poskanzer, H.G. Ritter, and R. Schicker, Proceedings of the Conference on Gross Properties of Nuclei and Nuclear Reactions, Hirschegg, 1989 (unpublished).
[33]K.G.R. Doss, H.Å. Gustafsson, H. Gutbrod, J.W. Harris, B.V. Jacak, K.H. Kampert, B. Kolb, A.M. Poskanzer, H.G. Ritter, H.R. Schmidt, L. Teitelbaum, M. Tincknell, S. Weiss, and H. Wieman, Phys. Rev. Lett. **59**, 2720 (1987).
[34]Christoph Hartnack, Diploma thesis, Institut für Theoretische Physik, Frankfurt (1989).

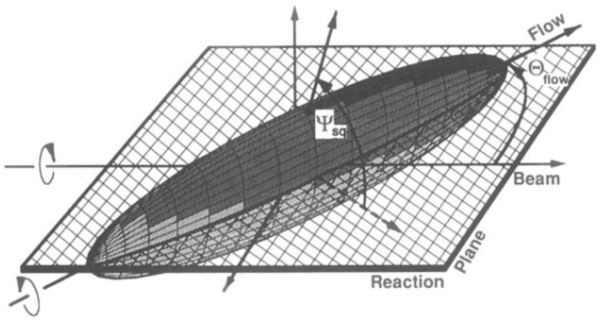

FIG. 3. A perspective view of a tri-axial ellipsoid. The major flow axis and the beam axis define the polar flow angle, θ_{flow}, and the reaction plane. The squeeze angle, ψ_{sq}, is defined as the azimuthal angle around the flow axis of the medium axis of the ellipsoid relative to the reaction plane.